



PAPER

 View Article Online
 View Journal | View Issue
Cite this: *RSC Adv.*, 2017, 7, 18224

Rapid, stable and self-powered perovskite detectors *via* a fast chemical vapor deposition process†

 Guoqing Tong,^a Xiangshun Geng,^b Yongqiang Yu,^b Linwei Yu,^a  ^{*a} Jun Xu,^a Yang Jiang,^b  ^{*b} Yun Sheng,^c Yi Shi^a and Kunji Chen^a

Organometal halide perovskite materials are outstanding candidates not only for solar cells but also for photo-detection. In this work, we develop a well-controlled lower temperature (<120 °C) and fast chemical vapor deposition process (LFCVD) to fabricate photovoltaic detectors with a high speed response ($\tau_{\text{rise}}/\tau_{\text{fall}} \sim 460$ ns/940 ns) and a 3 dB-bandwidth above 0.9 MHz, which are the highest among those with a large active area (>0.1 cm²) without external power supply. Remarkably, the perovskite photovoltaic detectors demonstrate an excellent air-exposure stability for more than two months without particular encapsulation. These excellent performances are attributed to a well-controlled expansive gas–solid reaction and formation of perovskite crystallites that collide and pinch off the pinhole leakage paths at the grain boundaries. More importantly, the accumulated strain at the colliding grain boundaries leads to a selective evaporation of MAI during post-growth annealing, and thus passivate the local defects by the remnant PbI₂ layer. These results highlight the potential of LFCVD perovskite materials in developing ultra-fast and self-driven photovoltaic detectors with outstanding stability and scalability.

 Received 4th February 2017
 Accepted 21st March 2017

DOI: 10.1039/c7ra01430a

rsc.li/rsc-advances

Introduction

Organometal trihalide perovskites (CH₃NH₃PbX₃, where X = Cl, Br, I, or a mix halide) are emerging new hybrid semiconductors that have enabled a series of exciting optoelectronic applications, including high performance photovoltaics (PV),^{1–4} light-emission,^{5,6} lasing^{7,8} and sensing.^{9–13} Thanks to a strong broad spectral absorption, a long carrier lifetime and a very high carrier mobility (≈ 10 cm² V^{−1} s^{−1}), the power conversion efficiency of the perovskite solar cells has reached a new record of 20.8%,^{14–16} and 22.1% very recently.¹⁷ In parallel, perovskite materials are promising candidates for rapid photodetections, operating in the visible and near infrared (NIR) spectrum range. For example, Hu Xin and Xie Yi *et al.* first reported a flexible organic-halide photodetector by one-step solution deposition and exhibited excellent flexibility and reasonable sensitivity.⁹ Yang Yang *et al.* demonstrated perovskite photodetectors working at low or even zero bias, with a fast response ($\tau_{\text{rise}}/\tau_{\text{fall}} \sim 0.97$ μs/1.1 μs), a large dynamic linear response up to 100 dB

and a detectivity approaching 10¹² Jones.¹⁰ Meanwhile, a high gain (nearly 500) perovskite detector has been achieved by Huang's group at a low driving or bias voltage of −1 V.¹²

Seeking a low-cost, scalable and reliable fabrication of the perovskite solar cells has been crucial to establishing large-scale photovoltaic and detector applications.^{18–20} All solution-based one-step or two-step spin-coating^{21–24} deposition are convenient strategies, but usually experience a radical reaction that is hard to control over large area. Alternatively, perovskite thin film can be deposited *via* sequential^{25,26} or concurrent^{15,27} thermal evaporations in expensive high vacuum system, where a precise and readily controllable deposition has been achieved. Recently, a vapor-assisted solution process (VASP),^{28–30} low pressure VASP (LPVASP),^{19,31} hybrid chemical vapor deposition (HCVD)^{32,33} and hybrid physical–chemical vapor deposition (HPCVD)³⁴ have been proposed to combine the solution-based fabrication with a low vacuum deposition and obtained a high performance in perovskite solar cells.

In this work, we explore a well-controlled lower temperature and fast chemical vapour deposition (LF-CVD) process within 20 min to prepare high quality compact perovskite films, and employ them in a vertical photodetector structure of FTO/c-TiO₂/CH₃NH₃PbI₃/Spiro-OMeTAD/Ag that exhibits very high speed detection with a response time of $\tau_{\text{rise}}/\tau_{\text{fall}} \sim 460$ ns/940 ns, a responsivity of 0.55 A W^{−1} and a 3 dB bandwidth above 0.9 MHz (the highest among those with a reasonable active area >0.1 cm²) without exterior power supply. Remarkably, all these have been achieved with an excellent air-exposure stability for

^aNational Laboratory of Solid State Microstructures, School of Electronics Science and Engineering, Collaborative Innovation Centre of Advanced Microstructures, Nanjing University, Nanjing 210093, China. E-mail: yulinwei@nju.edu.cn

^bSchool of Materials Science and Engineering, Hefei University of Technology, Hefei 230009, P. R. China. E-mail: apjiang@hfut.edu.cn

^cState Key Lab of Photovoltaic Science and Technology, Trina Solar, Changzhou 213031, P. R. China

† Electronic supplementary information (ESI) available. See DOI: 10.1039/c7ra01430a



The LFCVD setup and the fabrication procedure are schematically illustrated in the Fig. 1a. First, a PbI_2 thin film was spin-coated on transparent FTO/c- TiO_2 substrates. Then, the sample was loaded into a high-vacuum tube furnace in zone II, while MAI ($\text{CH}_3\text{NH}_3\text{I}$) powder in crucible were placed in the upstream in zone I. Note that, the temperatures at different zones can be independently controlled, and the base vacuum in the tube is pumped to 10^{-3} Pa by turbo molecular pump. Upon heating to $\sim 120^\circ\text{C}$ in zone I, the MAI powder starts to evaporate,^{19,32} and carried by 100 SCCM Ar gas to transport over zone II loaded with PbI_2 substrates. During the reaction, the temperature of zone II was kept at 100°C for 20 min. After that, the samples were in-suit annealed in zone II to remove the excess MAI on the surface. Finally, photovoltaic devices (Fig. 1b) were fabricated following the standard procedures as detailed in the Experiments section.

The typical SEM images of the perovskite thin films, before and after annealing at 90 °C, 120 °C and 150 °C, are shown in Fig. 2a–d, respectively. As we can see, the as-prepared perovskite thin film features a compact array of faceted grains with a size of 200–300 nm and a full coverage over the FTO/c-TiO₂ glass substrate. After annealing at 90 °C for 30 min in air (see Fig. 2b),

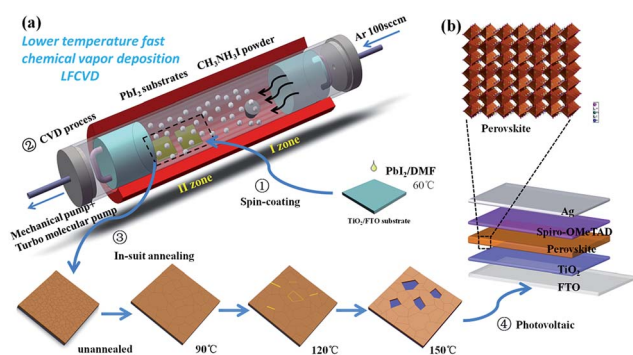


Fig. 1 (a) Schematic diagram of the configuration of the two-temperature-zones furnace tube and the fabrication procedure of a lower temperature fast chemical vapor deposition process (LFCVD) for synthesizing perovskite ($\text{CH}_3\text{NH}_3\text{PbI}_3$) films. (b) The multilayer structure of the final perovskite photovoltaic detector.

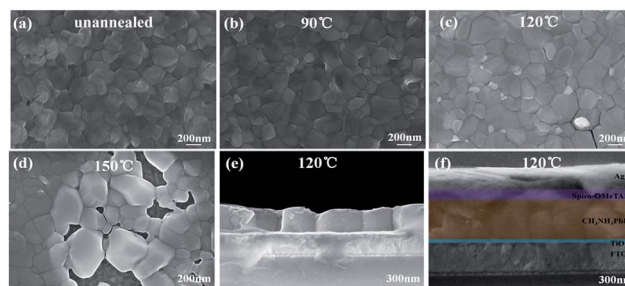


Fig. 2 SEM images of the perovskite films deposited *via* LFCVD procedure on FTO/c-TiO₂, (a) before and after annealing at (b) 90 °C, (c) 120 °C and (d) 150 °C for 30 min, respectively. The cross-section SEM image of (e) the perovskite film after annealing at 120 °C for 30 min, (f) the multilayer structure in a complete photovoltaic structure.

the perovskite grains become smoother on the surface and slightly larger in grain size. Increasing the annealing temperature to 120 °C, bright spots appear among the perovskite grains, as witnessed in Fig. 2c, which could be assigned to the decomposition of perovskite back into PbI_2 crystals at higher temperature annealing.^{35–37} Annealing at even higher temperature to 150 °C causes significant damage of the integrity of perovskite thin film, as witnessed in the SEM image shown in Fig. 2d, where large holes and huge grains appear from place to place.

The disintegration of perovskite thin film back into PbI_2 upon higher temperature post-growth annealing can be inferred from the XRD analysis of the samples plotted in Fig. 3a, where the sharp diffraction peaks found at 12.62° after annealing at 120°C and 150°C indicate the formation of PbI_2 crystals.^{19,38} Meanwhile, the absorption spectra of the corresponding samples, as seen in Fig. 3b, show that the annealing temperature ramping causes first an increase of the absorbance after 90°C or 120°C , and then drop quickly at high temperature

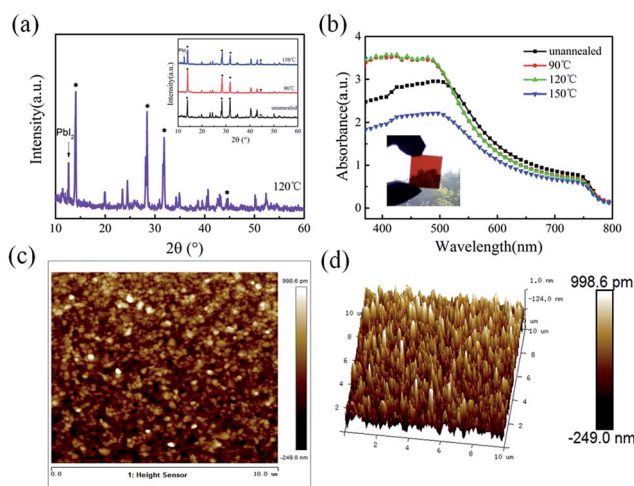


Fig. 3 (a) XRD patterns and (b) the absorption spectra of the $\text{CH}_3\text{-NH}_3\text{PbI}_3$ thin films after annealing at different temperature, respectively. (c) 2D, (d) 3D AFM characterizations of the LFCVD $\text{CH}_3\text{NH}_3\text{PbI}_3$ thin film after annealing at 120 °C on the FTO/c- TiO_2 substrate.

where i_n is the noise current and R the responsivity. The noise current was measured at various frequency under dark condition with a lock-in amplifier (SR830). As shown in Fig. 4c, the noise current declines with the increase of modulation frequency, and reach $2.2 \text{ pA Hz}^{-1/2}$ at 700 Hz under zero bias. Thus, the NEP is estimated to be $4 \times 10^{-12} \text{ W Hz}^{-1/2}$, which is comparable to that achieved in the best all-solution-processed perovskite photodetector.¹⁰

Besides, the characteristic response times of the perovskite photodetectors are also extracted under different modulation frequency ranging from 100 Hz to 4 MHz by a function generator. As shown in Fig. 5a, the perovskite device exhibits an excellent stability and reproducibility at 30 kHz, 300 kHz and 800 kHz modulated light signals, even up to 2.5 MHz (as seen Fig. S4†), which is even higher than that reported in the literature based on nanoribbons (NR) Schottky barrier diodes (500 Hz) and MoS_2 -based photodetectors (3.3 kHz).^{41–43} The rise time (τ_r) and fall time (τ_f), defined as the rising interval (from 10% to 90% of the maximum) and the falling (from 90% to 10%), are determined to be 460 ns and 940 ns at 300 kHz modulation, respectively. In addition, at 1 MHz, the rise and fall times degrade to 350 ns and 470 ns, but still with a clear waveform output against the noise background, as witnessed in Fig. S4 and S5 (ESI†).

→ Remarkably, we found that the post-annealing also has a very important influence to the photo-response speeds of the perovskite detectors. As seen in Fig. S6 in the ESI† materials, the rise/fall time scales of the original perovskite detector and those annealed at lower (90 °C) or higher (150 °C) temperature, all degrade to 3.7 μs /4.0 μs , 1.1 μs /1.4 μs and 0.8 μs /3.1 μs , respectively, compared to that of 0.46 μs /0.94 μs achieved at optimal annealing at 120 °C. This is because the response time is closely related to the electric quality of the overall perovskite thin film junction. As the perovskite film annealed at 150 °C suffers from a larger current leakage due to the formation of pinholes and voids, the responsive photocurrent signals (that require a build-up progress for an effective read-out in the outer circuit) have to first compensate for this portion of current loss,

and thus leading to a slower response. On the other hand, for the original or insufficient annealing at 90 °C, the crystalline quality of the perovskite grains is inferior to that obtained at 120 °C annealing, and thus the photo-carrier transport in the perovskite junction is slower, also limiting the speed of photo-detection. Only the optimized annealing at 120 °C is sufficient and right to improve the grain quality while maintain an integrity of the thin film, as a key basis to achieve a rapid response in photodetection.

In comparison to the other perovskite-based PDs, few-layer MoS_2 photodetectors and quantum dot photodetectors, as summarized in Table 1^{10,12,13,44–49} our perovskite photodetectors fabricated with a well-controlled LFCVD process demonstrate the fastest response, thanks to a high quality and compact perovskite thin film formation and the beneficial passivation effect of the remnant PbI_2 at the grain boundaries, as will be discussed later. More importantly, as seen in Table 1, our LFCVD-processed perovskite photodetector has achieved an excellent 3 dB bandwidth, the highest one among those with a reasonably large active area (close to 0.1 cm^2).^{10,11} Note that, the bandwidth $f_{3\text{dB}}$ is predicted to increase significantly when the area decreases because the 3 dB bandwidth and the response speed are coupled to the resistor-capacitor (RC) constants of the circuitry.

Finally, the stability of perovskite devices has been a critical issue that limits their practical applications. Surprisingly, we found that the photodetectors fabricated *via* such a mildly-controlled LFCVD exhibited a good stability without encapsulation in the air. As shown in Fig. 6, after a lasting exposure in air (25 °C, RH \sim 40%) up to 60 days, a clear response to the modulated light signals has been maintained for the perovskite photodetectors. Although the device degrade gradually in terms of rise time, from 0.46 μs to 5.22 μs , particularly pulled down by fall time from 0.94 μs to only 9.04 μs , the response time still faster than most of previous reports, as summarized in Table 1. The deterioration is in general ascribed to the disintegration of Spiro-MeOTAD layer that will happen inevitably in contact with moisture in air.⁵⁰ Notably, our results provide the first ever experimental proof for the stability issue of the LFCVD-based perovskite photodetectors. One of the reasons could be that this gently controlled vapor deposition and reaction process allows a thorough removal of the residual solvents and thus promotes a high quality crystallization of compact perovskite grains, reducing the metastable phases among the thin films.^{20,28}

As schematically depicted in Fig. 1b, the LFCVD process allows a milder gas-solid reaction and sufficient time for the MAI vapor to react with the PbI_2 crystals, not only on the surface but also deep into the boundary regions among the crystals, which is the key to achieve a uniform and compact perovskite film. This has been supported by the cross-section SEM observation of the LFCVD perovskite thin film after 120 °C annealing presented in Fig. 2e, where all the grain boundary lines are mostly aligned in the normal direction to the substrate, as a result of a strong collision and squeezing among the neighboring expanding grains during the gas-solid reaction. This thus helps to pinch off the pinholes at the grain boundaries, not

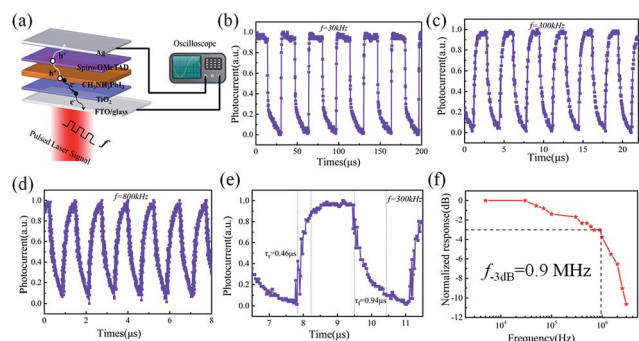


Fig. 5 Schematic illustration of the perovskite device to measure photo-response speed. Time response characteristics of the device under different pulsed light illumination (a) perovskite device under pulsed light illumination (650 nm), (b) 30 kHz, (c) 300 kHz, (d) 800 kHz. (e) The magnified and normalized plots of one response cycle 300 kHz. (f) 3 dB bandwidth of perovskite device.



Device	Preparation process	Active area [cm ²]	Rise/fall time [μs]	Bandwidth (f _{3dB}) [MHz]	Ref.
FTO/TiO₂/perovskite/Spiro-OMeTAD/Ag	LFCVD	0.1	0.46/0.94	0.9	This work
ITO/perovskite/TPD-Si/MoO ₃ /Ag	Solution	0.06	5.7/41	—	12
FTO/TiO ₂ /Al ₂ O ₃ /PCBM/perovskite/Spiro-OMeTAD/Au/Ag	Solution	0.07	1/3	—	13
FTO/TiO ₂ /perovskite/Spiro-OMeTAD/Au	Solution	0.16	17/20	—	44
ITO/PEDOT:PSS/perovskite/PC ₆₀ BM/C ₆₀ /LiF/Ag	Solution	0.2	1.7/1	0.5	45
ITO/PEDOT:PSS/perovskite/PCBM/Al	Solution	0.1	0.97/1.1	0.8	10
		0.01		2.9	
ITO/PTAA/perovskite/C ₆₀ /BCP/Cu	Solution	0.07	0.115 ^a	—	51
ITO/OTPD/perovskite/PCBM/C ₆₀ /BCP/Al	Solution	0.07	0.28 ^a	2.9	11
Au/perovskite/Au	Solution	—	300/300	—	46
WS ₂ /perovskite heterojunction	Vapor	—	2.7/7.5	—	47
MoS ₂ /Si heterojunction	—	—	3/40	—	48
In/Ga/n-SiNW/CQDs/Au	—	—	20/40	—	49

This journal is © The Royal Society of Chemistry 2017

optimal annealing at 120 °C. This can be attributed to the fact that the residual PbI_2 passivation at the grain boundary help to passivate and reduce the recombination centres in the perovskite thin films, and thus a longer photo-carrier lifetime and higher population contribute to a higher photo-current response in the I - V measurement.

Most importantly, as mentioned above, the devices without annealing and annealing at 90 °C and 150 °C show a poor response time estimated to 3.7 μs /4.0 μs , 1.1 μs /1.4 μs and 0.8 μs /3.1 μs , respectively, which is much more slowly than that annealing at 120 °C (0.46 μs /0.94 μs). It indicates that the defect in the film and boundary, to some extent, block the transportation of the exciton and increase the recombination chance, leading to a long response time. These results support that the PbI_2 provides a good passivation to the boundary to reduce the recombination centre and effectively increases the photocurrent and improve the response time, leading to a high performance of perovskite photodetector.

Conclusions

In summary, we have demonstrated a well-controlled LFCVD fabrication of high quality perovskite thin film that enables high performance and stable self-sustained photodetector application. The photovoltaic devices under 120 °C annealing for 30 min achieve a PCE as high as 15.1%. Photodetector exhibits a responsivity of 0.55 A W^{-1} , detectivity up to $\sim 10^{12}$ Jones, a fast response (with rise and fall times of 460 ns/940 ns) and a wide 3 dB bandwidth up to 0.9 MHz, with outstanding stability to 60 days air exposure. We propose that the accumulated strain at the colliding grain interfaces leads to a selective formation of PbI_2 layer at the grain boundaries that help to passivate local recombination centers and block local current leakage. These benefits combined indicate a new and reliable manufacturing of high performance self-driven photovoltaic and photodetector applications.

Acknowledgements

This work was financed by Scientific and Technological Support Programme in Jiangsu province under No. BE2014147-2, NSFC under No. 61674075, 11274155, 61204050, U1632151, Open Research Fund of State Key Laboratory of Pulsed Power Laser Technology of China (Hefei, SKL 2015 KF 04), JSNSFC No. BK20150275, Jiangsu Shuangchuang Team's and Personal Program, Jiangsu Excellent Young Scholar Program and the Fundamental Research Funds for the Central Universities.

Notes and references

- 1 Y. Zhao and K. Zhu, *Chem. Soc. Rev.*, 2016, **45**, 655–689.
- 2 O. Malinkiewicz, A. Yella, Y. H. Lee, G. M. Espallargas, M. Graetzel, M. K. Nazeeruddin and H. J. Bolink, *Nat. Photonics*, 2014, **8**, 128–132.
- 3 H. T. Wanyi Nie, R. Asadpour, J.-C. Blancon, A. J. Neukirch, G. Gupta, J. J. Crochet, M. Chhowalla, S. Tretiak,

- M. A. Alam, H.-L. Wang and A. D. Mohite, *Science*, 2015, **347**, 522–525.
- 4 B. Li, Y. Li, C. Zheng, D. Gao and W. Huang, *RSC Adv.*, 2016, **6**, 38079–38091.
- 5 O. A. Jaramillo-Quintero, R. S. Sanchez, M. Rincon and I. Mora-Sero, *J. Phys. Chem. Lett.*, 2015, **6**, 1883–1890.
- 6 Z. K. Tan, R. S. Moghaddam, M. L. Lai, P. Docampo, R. Higler, F. Deschler, M. Price, A. Sadhanala, L. M. Pazos, D. Credginton, F. Hanusch, T. Bein, H. J. Snaith and R. H. Friend, *Nat. Nanotechnol.*, 2014, **9**, 687–692.
- 7 Q. Zhang, S. T. Ha, X. Liu, T. C. Sum and Q. Xiong, *Nano Lett.*, 2014, **14**, 5995–6001.
- 8 F. Deschler, M. Price, S. Pathak, L. E. Klintberg, D. D. Jarausch, R. Higler, S. Hüttner, T. Leijtens, S. D. Stranks, H. J. Snaith, M. Atature, R. T. Phillips and R. H. Friend, *J. Phys. Chem. Lett.*, 2014, **5**, 1421–1426.
- 9 X. Hu, X. Zhang, L. Liang, J. Bao, S. Li, W. Yang and Y. Xie, *Adv. Funct. Mater.*, 2014, **24**, 7373–7380.
- 10 L. Dou, Y. M. Yang, J. You, Z. Hong, W. H. Chang, G. Li and Y. Yang, *Nat. Commun.*, 2014, **5**, 5404.
- 11 Y. Fang and J. Huang, *Adv. Mater.*, 2015, **27**, 2804–2810.
- 12 R. Dong, Y. Fang, J. Chae, J. Dai, Z. Xiao, Q. Dong, Y. Yuan, A. Centrone, X. C. Zeng and J. Huang, *Adv. Mater.*, 2015, **27**, 1912–1918.
- 13 B. R. Sutherland, A. K. Johnston, A. H. Ip, J. Xu, V. Adinolfi, P. Kanjanaboos and E. H. Sargent, *ACS Photonics*, 2015, **2**, 1117–1123.
- 14 D. B. W. Tress, M. I. Dar, P. Gao, J. Luo, C. Renevier, K. Schenk, A. Abate, F. Giordano, J. P. Correa Baena, J. D. Decoppet, S. M. Zakeeruddin, M. K. Nazeeruddin, M. Grätzel and A. Hagfeldt, *Sci. Adv.*, 2016, **2**, 1501170.
- 15 M. Liu, M. B. Johnston and H. J. Snaith, *Nature*, 2013, **501**, 395–398.
- 16 N. J. Jeon, J. H. Noh, W. S. Yang, Y. C. Kim, S. Ryu, J. Seo and S. I. Seok, *Nature*, 2015, **517**, 476–480.
- 17 National Renewable Energy Laboratory, Best Research Cell Efficiency, accessed: January, 2016, http://www.nrel.gov/ncpv/images/efficiency_chart.jpg.
- 18 H. S. Duan, H. Zhou, Q. Chen, P. Sun, S. Luo, T. B. Song, B. Bob and Y. Yang, *Phys. Chem. Chem. Phys.*, 2015, **17**, 112–116.
- 19 P. F. Luo, Z. F. Liu, W. Xia, C. C. Yuan, J. G. Cheng and Y. W. Lu, *ACS Appl. Mater. Interfaces*, 2015, **7**, 2708–2714.
- 20 X. Li, D. Bi, C. Yi, J.-D. Decoppet, J. Luo, S. M. Zakeeruddin, A. Hagfeldt and M. Grätzel, *Science*, 2016, **353**, 58–62.
- 21 H. Zhou, Q. Chen, G. Li, S. Luo, T.-b. Song, H.-S. Duan, Z. Hong, J. You, Y. Liu and Y. Yang, *Science*, 2014, **345**, 542–546.
- 22 D. Liu and T. L. Kelly, *Nat. Photonics*, 2013, **8**, 133–138.
- 23 N. J. Jeon, J. H. Noh, Y. C. Kim, W. S. Yang, S. Ryu and S. I. Seok, *Nat. Mater.*, 2014, **13**, 897–903.
- 24 J. Burschka, N. Pellet, S.-J. Moon, R. Humphry-Baker, P. Gao, M. K. Nazeeruddin and M. Grätzel, *Nature*, 2013, **499**, 316–319.
- 25 A. Ng, Z. Ren, Q. Shen, S. H. Cheung, H. C. Gokkaya, G. Bai, J. Wang, L. Yang, S. K. So, A. B. Djurišić, W. W.-f. Leung,



- J. Hao, W. K. Chan and C. Surya, *J. Mater. Chem. A*, 2015, **3**, 9223–9231.
- 26 C. W. Chen, H. W. Kang, S. Y. Hsiao, P. F. Yang, K. M. Chiang and H. W. Lin, *Adv. Mater.*, 2014, **26**, 6647–6652.
- 27 O. Malinkiewicz, A. Yella, Y. H. Lee, G. M. Espallargas, M. Graetzel, M. K. Nazeeruddin and H. J. Bolink, *Nat. Photonics*, 2013, **8**, 128–132.
- 28 Q. Chen, H. Zhou, Z. Hong, S. Luo, H. S. Duan, H. H. Wang, Y. Liu, G. Li and Y. Yang, *J. Am. Chem. Soc.*, 2014, **136**, 622–625.
- 29 C. Liu, J. Fan, X. Zhang, Y. Shen, L. Yang and Y. Mai, *ACS Appl. Mater. Interfaces*, 2015, **7**, 9066–9071.
- 30 J. Mao, H. Zhang, H. He, H. Lu, F. Xie, D. Zhang, K. S. Wong and W. C. H. Choy, *RSC Adv.*, 2015, **5**, 73760–73766.
- 31 Y. Li, J. K. Cooper, R. Buonsanti, C. Giannini, Y. Liu, F. M. Toma and I. D. Sharp, *J. Phys. Chem. Lett.*, 2015, **6**, 493–499.
- 32 M. R. Leyden, M. V. Lee, S. R. Raga and Y. Qi, *J. Mater. Chem. A*, 2015, **3**, 16097–16103.
- 33 M. R. Leyden, L. K. Ono, S. R. Raga, Y. Kato, S. Wang and Y. Qi, *J. Mater. Chem. A*, 2014, **2**, 18742–18745.
- 34 Y. Peng, G. Jing and T. Cui, *J. Mater. Chem. A*, 2015, **3**, 12436–12442.
- 35 Q. Chen, H. Zhou, T. B. Song, S. Luo, Z. Hong, H. S. Duan, L. Dou, Y. Liu and Y. Yang, *Nano Lett.*, 2014, **14**, 4158–4163.
- 36 G. Rajendra Kumar, A. Dennyson Savariraj, S. N. Karthick, S. Selvam, B. Balamuralitharan, H. J. Kim, K. K. Viswanathan, M. Vijaykumar and K. Prabakar, *Phys. Chem. Chem. Phys.*, 2016, **18**, 7284–7292.
- 37 G. E. Eperon, V. M. Burlakov, P. Docampo, A. Goriely and H. J. Snaith, *Adv. Funct. Mater.*, 2014, **24**, 151–157.
- 38 T. Supasai, N. Rujisamphan, K. Ullrich, A. Chemseddine and T. Dittrich, *Appl. Phys. Lett.*, 2013, **103**, 183906.
- 39 K. N. Liang, D. B. Mitzi and M. T. Prikas, *Chem. Mater.*, 1998, **10**, 403.
- 40 X. Geng, Y. Yu, X. Zhou, C. Wang, K. Xu, Y. Zhang, C. Wu, L. Wang, Y. Jiang and Q. Yang, *Nano Res.*, 2016, 1–11.
- 41 J. P. Lu, J. Lu, H. Liu, B. Liu, K. X. Chan, J. Lin, W. Chen, K. P. Loh and C. H. Sow, *ACS Nano*, 2014, **8**, 6334–6343.
- 42 W. Choi, M. Y. Cho, A. Konar, J. H. Lee, G. B. Cha, S. C. Hong, S. Kim, J. Kim, D. Jena, J. Joo and S. Kim, *Adv. Mater.*, 2012, **24**, 5832–5836.
- 43 D. Wu, Y. Jiang, Y. Zhang, Y. Yu, Z. Zhu, X. Lan, F. Li, C. Wu, L. Wang and L. Luo, *J. Mater. Chem.*, 2012, **22**, 23272–23276.
- 44 D. Li, G. Dong, W. Li and L. Wang, *Sci. Rep.*, 2015, **5**, 7902.
- 45 Q. Lin, A. Armin, D. M. Lyons, P. L. Burn and P. Meredith, *Adv. Mater.*, 2015, **27**, 2060–2064.
- 46 H. Deng, X. Yang, D. Dong, B. Li, D. Yang, S. Yuan, K. Qiao, Y. B. Cheng, J. Tang and H. Song, *Nano Lett.*, 2015, **15**, 7963–7969.
- 47 C. Ma, Y. Shi, W. Hu, M. H. Chiu, Z. Liu, A. Bera, F. Li, H. Wang, L. J. Li and T. Wu, *Adv. Mater.*, 2016, **28**, 3683–3689.
- 48 L. Wang, J. Jie, Z. Shao, Q. Zhang, X. Zhang, Y. Wang, Z. Sun and S.-T. Lee, *Adv. Funct. Mater.*, 2015, **25**, 2910–2919.
- 49 C. Xie, B. Nie, L. H. Zeng, F. X. Liang, M. Z. Wang, L. B. Luo, M. Feng, Y. Q. Yu, C. Y. Wu, Y. C. Wu and S. H. Yu, *ACS Nano*, 2014, **8**, 4015–4022.
- 50 L. K. Ono, M. R. Leyden, S. Wang and Y. Qi, *J. Mater. Chem. A*, 2016, **4**, 6693–6713.
- 51 L. Shen, Y. Fang, D. Wang, Y. Bai, Y. Deng, M. Wang, Y. Lu and J. Huang, *Adv. Mater.*, 2016, **28**, 10794–10800.

